A Simple Model for the Prediction of the Ballistic Limit in Thick-section Composite Laminates

M. Grujicic [*1], J. S. Snipes, N. Chandrasekharan

Department of Mechanical Engineering, Clemson University Clemson, SC 29634, USA

[*1]gmica@clemson.edu

Abstract

In the present work, an attempt is made to develop a simple semi-empirical model for prediction of the ballistic-limit of thick-section composite laminates when subjected to a normal impact by a solid (right circular cylinder) projectile (made of a hard enough material to resist plastic deformation). Towards that end, the projectile/composite-laminate interaction process is divided into three distinct phases: (a) a short-term, shock-wave dynamics controlled (initial) Phase 1; (b) a relatively-longer, composite-laminate material deformation/damage/failure controlled (intermediate) Phase 2; and (c) a structural-vibration dominated (final) Phase 3. Projectile/composite-laminate interaction within Phase 1 is analyzed using the theory of planar, longitudinal shock-waves which yielded the reactive force acting on the projectile as a function of the projectile forward displacement. Within the interaction Phases 2 and 3, on the other hand, the reactive force vs. projectile forward displacement relation is obtained using the results (properly modified to include the dynamic effects) of quasi-static punch-shear tests (at varying support-span over punch-diameter ratios). The ballistic-limit results yielded by the model are compared with their finite-element analysis counterparts and a reasonable agreement is observed.

Keywords

Thick Composite Laminates; Ballistic-limit Prediction; Modeling and Simulation

Introduction

The subject of the present work is high specific-strength and high specific-stiffness fiber-reinforced (e.g. S-2 Glass, Kevlar® etc.) polymer-matrix composite-laminate materials and structures. These materials/structures are commonly used in various protective systems whose main requirement is a high level of mass-efficient penetration resistance against high kinetic energy projectiles (e.g. bullets, mine, IED or turbine fragments, etc.). These protection systems are traditionally developed using legacy knowledge and their development relies extensively on the use of a fabricate-and-test approach. Since this approach is not only economically unattractive, but is often associated with significantly longer lead times, it has gradually become complemented by the appropriate cost- and time-efficient Computer Aided Engineering (CAE) analyses. This trend has been accelerated by the recent developments in the numerical modeling of transient non-linear dynamics phenomena such as those accompanying ballistic and blast loading conditions (e.g. Grujicic *et al.*, 2007b, 2008a, b, c, 2010a). However, the tools used in these analyses themselves suffer from a number of shortcomings/limitations which prevent these analyses from being more widely utilized. One of the main shortcomings stems from the fact that these analyses entail knowledge of the accurate material models which, with high fidelity, must account for the response of projectile/target materials under high-deformation rate, large-strain, high-pressure loading conditions (conditions typically encountered during ballistic/blast impact events). Development of such material models is itself a tedious and costly process and, hence, there is a perceived need for relatively simple, semi-empirical computational models/procedures which can be used for prediction of the protective-structure ballistic-resistance/limit, while not requiring all the constitutive-behavior details of the materials involved. In the present work, an attempt is made to develop such a simple, semi-empirical computational model/procedure for the case of a (plastically non-deformable) projectile impacting a thick-section composite-laminate (target armor) structure. In these composite-laminate structures, projectile/target interactions are, at least in the earlier stages of interactions, controlled by the through-the-thickness shear-based phenomena and less affected by the bending of the target. In thin-section target structures, in sharp contrast, bending plays a more pronounced

role and these armor structures are outside the scope of the present work. Hence, while the adjective "thick-section" will be mainly omitted in the remainder of this manuscript, it should be noted that the analysis developed and the results obtained pertain exclusively to the case of thick-section composite laminates.

As will be discussed in greater detail in the remainder of this section and in Section II, the projectile/composite-laminate interaction process can be divided into several distinct (consecutive) stages which could be grouped into three main phases: (a) a short-term, shock-wave dynamics controlled (initial) Phase 1; (b) a relatively longer, composite-laminate material deformation/damage/failure controlled (intermediate) Phase 2; and (c) a structural-vibration dominated (final) Phase 3, whose duration is controlled by the severity of impact and the extent of material/structural damping. The analysis of projectile/composite-laminate interaction Phase 1, based on the theory of planar longitudinal shock-waves is one of the main objectives of the present work and will be presented in Section II. On the other hand, Phases 2 and 3 will be modeled using the experimental procedures and results (modified to include dynamic effects) obtained in the open literature using the conventional (quasi-static) punch-shear tests (at varying support-span over punch-diameter ratios). As will be discussed later in this section, by means of the implementation of the (quasi-static) punch-shear tests at different values of the support-span over punch-diameter ratio, insight can be gained into the constitutive response of the composite-laminate structures under ballistic-impact conditions at different stages of projectile penetration.

Based on the foregoing discussion, the topics which need to be covered in remainder of this section include: (a) the main composite-laminate dynamic deformation/damage/failure penetration stages under ballistic loading conditions; and (b) the (quasi-static) punch shear testing procedure and its use in identifying and quantifying the main composite-laminate dynamic deformation/damage/failure penetration stages. These topics are briefly reviewed in the remainder of this section.

Projectile/Composite-laminate interaction stages: Based on the work of Zhou and Davies (1995), the work of Bless and Hartman (1989), the work of Gama and Gillespie (2008), and the work of Haque and Gillespie (2012) in which extensive investigations of the ballistic-impact and penetration behavior of thick-section E-glass/polyester composites were carried out, the following five projectile/composite-laminate (consecutive) interaction stages can be identified:

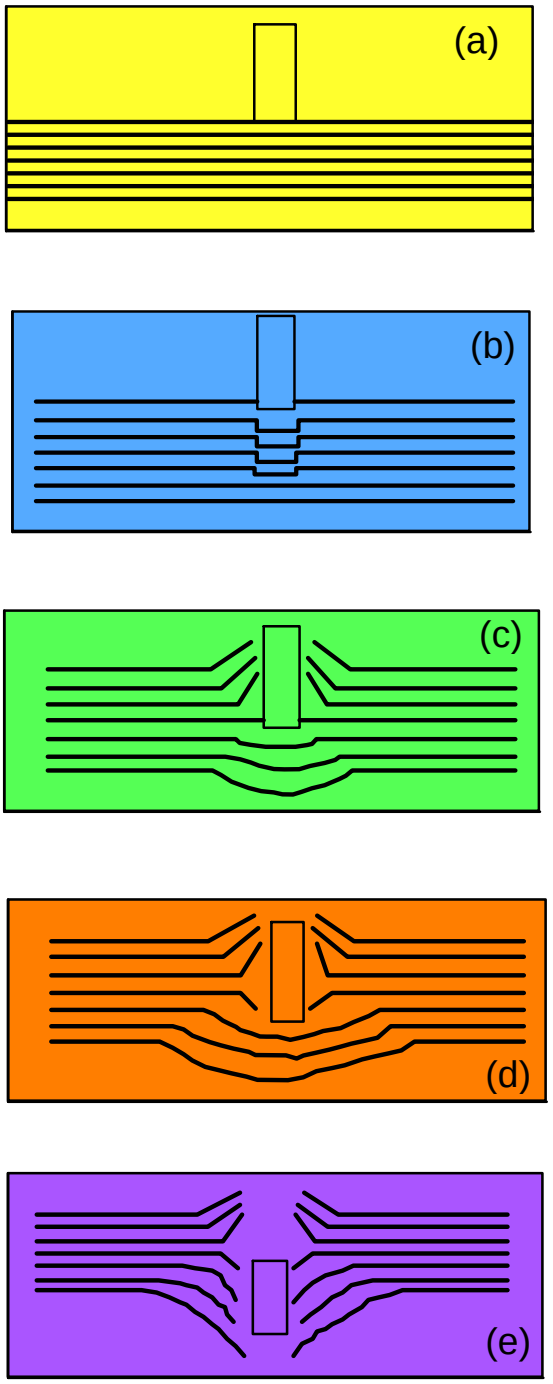

FIG. 1. FIVE BASIC STAGES OF THE PENETRATION OF THICK-SECTION COMPOSITE LAMINATES BY A (PLASTICALLY NON-DEFORMABLE) PROJECTILE. PLEASE SEE TEXT FOR DETAILS.

(a) An initial "*dwelling*" impact stage which is controlled by the propagation of shock-waves within the projectile and the composite-laminate and within which no noticeable projectile penetration is detected, as shown in Figure 1(a);

(b) An initial stage of projectile penetration, which is characterized by large through-the-thickness shear in the presence of high hydrostatic compression, as shown in Figure 1(b). These loading conditions lead to the damage and failure of the fibers and matrix around the rim and underneath the projectile. Within this stage, a growing "cone of influence" is generated within the composite-laminate. It is important to note that, only the material within the cone is affected by, the (ballistic) loading;

(c) A "*shear-plug*" formation stage within which the cone of influence has fully extended to the composite-laminate back-face, as shown in Figure 1(c). As the shear-plug is being pushed out by the advancing projectile, the conical geometry of the plug gives rise to a reduction in lateral compression;

(d) A stage within which through-the-thickness shearing continues, but the hydro-dynamic component of the stress field becomes tensile (due to combined effects of composite-laminate bending and shock-wave reflection from the composite-laminate back-face), as shown in Figure 1(d); and,

(e) A final stage of (complete or incomplete) penetration within which the projectile/composite-laminate interaction is characterized by extensive vibrations, as shown in Figure 1(e).

As mentioned above, for practical purposes, the five interaction stages are regrouped into three interaction phases where the letters respectively contain stages 1, 2–4, and 5.

The (quasi-static) punch shear testing procedure: The discussion presented in the previous section revealed that, during a ballistic-impact, a cone of influence is formed within the composite-laminate target structure. This cone grows in the lateral directions as the projectile penetrates the target and, it should be recalled that, only the material within the cone is affected by, the (ballistic) loading. In other words, the material outside the cone is not affected by the projectile impact and acts solely as a lateral support. Consequently, as the cone grows during the advancement of the projectile through the target, the span of the supporting material increases.

Dynamic-impact tests within which a projectile is propelled towards, and impacts the composite-laminate target at, a high velocity are suitable in determining the ballistic resistance/limit of the target structure. Such a resistance/limit is often defined using the velocity, V_{50} , i.e., a velocity at which the probability for full penetration is 50 percent. However, the dynamic-impact tests typically require costly experimental setups. In addition, these tests do not provide any information about the force opposing the advancement of the projectile into the target as a function of the projectile penetration depth (or as a function of the projectile forward displacement). To overcome these limitations of the dynamic-impact tests, Gama and Gillespie (2008) and Haque and Gillespie (2012) proposed the use of quasi-static punch-shear tests. To account for the afore-mentioned increase in the span with an increase in projectile forward displacement, Gama and Gillespie (2008) and Haque and Gillespie (2012) suggested that the quasi-static punch-shear tests should be carried out at different values of span/punch-diameter ratio.

A schematic of a typical quasi-static punch-shear test apparatus is depicted in Figure 2(a). Starting from the bottom portion of this figure, the following main components of the apparatus can be identified: (a) a square frame made of square-cross-section welded steel tubes, bolted to the rigid work bench; (b) a heavy gage steel plate, bolted to the frame. The plate contains a circular through-the-thickness hole whose diameter defines the span. In the zero-span case, corresponding to the initial penetration stage accompanied by shear and hydrostatic compression, the heavy gage steel support plate doesn't contain a circular hole; (c) a thinner gage steel plate with a circular hole slightly larger than the punch cross-section; and (d) a cylindrical punch attached to the cross-head of a mechanical testing machine (or to another type of mechanical actuator).

An example of the typical quasi-static punch-shear results obtained from the work of Gama and Gillespie (2008) and the work of Haque and Gillespie (2012) is depicted in Figure 2(b). Individual force vs. punch displacement curves in this figure are denoted by their corresponding value of the span/punch-diameter ratio. Examination of the results displayed in Figure 2(b) reveals that: (a) with the exception of the span over the punch diameter ratio of 0.0, the punch force initially rises, at a relatively high rate, with an increase in the punch displacement. Then, after passing through a peak value, the punch force decreases parabolically towards its zero value; (b) the peak force decreases

with (a 0.0–4.0) increase in the span/punch-diameter ratio. This trend is inverted at even higher values (e.g. 8.0) of the span/punch-diameter ratio indicating a transition between the shear-dominated and bending-dominated punch/composite-laminate interactions; and (c) at a zero value of the span/punch-diameter ratio, the punch force increases linearly with the punch displacement up to the onset of penetration. At this point the punch force momentarily levels off before continuing to rise with an increase in the punch displacement.

In addition to carrying out the quasi-static punch-shear experiments, Gama and Gillespie (2008) and Haque and Gillespie (2012) conducted the corresponding ballistic tests. These tests were complimented by a series of extensive post-mortem examinations of the target plates documenting the type and the extent of damage in partially penetrated targets. They concluded that when the span support in the quasi-static and ballistic tests are matched, the deformation/damage/failure modes and their extent also match between the static and ballistic tests. Consequently, it is concluded that quasi-static punch-shear test results, after properly accounting for the additional dynamic effects, can be used to quantify the projectile/composite-laminate interactions in Phases 2 and 3. Additional details regarding the use of the quasi-static punch-shear results in the quantification of the composite-laminate ballistic limit are deferred to Section II.

Objectives: As mentioned earlier, the two main objectives of the present study are: (a) development of a simple semi-empirical computational model for the calculation of the ballistic limit in thick-section composite-laminates; and (b) validation of the model by comparing its predictions with their counterparts obtained in a companion three-dimensional transient non-linear dynamics finite-element analysis of the projectile/composite-laminate interaction.

Organization of the Paper: Details regarding the development of the present simple semi-empirical computational model for the prediction of thick-section composite-laminate ballistic limit are presented in Section II. Validation of this model through the comparison of its predictions with the corresponding predictions of a companion finite-element analysis is discussed in Section III. The key findings resulting from the present work are summarized in Section IV.

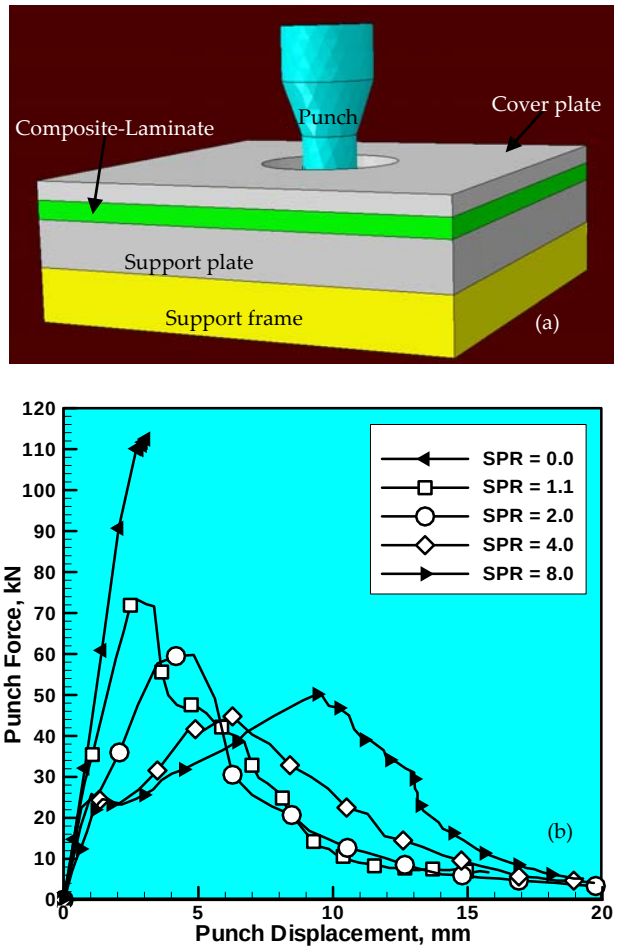

FIG. 2 (A) A SCHEMATIC OF A PROTOTYPICAL QUASI-STATIC PUNCH-SHEAR APPARATUS; AND (B) TYPICAL PUNCH-FORCE VS. PUNCH FORWARD DISPLACEMENT RESULTS OBTAINED AT DIFFERENT VALUES OF THE SPAN/PUNCH-DIAMETER RATIO (SPR).

Development and Application of the Model

The problem analyzed in this section involves a normal (zero obliquity angle) impact of a (solid, right circular cylinder) projectile onto a thick-section composite-laminate target structure. A schematic of this impact is shown in Figure 3(a). As mentioned earlier, previous experimental and finite-element computational investigations (e.g. Zhou and Davies, 1995; Bless and Hartman, 1989; Gama and Gillespie, 2008; Haque and Gillespie, 2012) established that the interaction of a projectile with a thick-section composite-laminate involves five distinct stages which were grouped, in the present work, into three distinct phases: (a) a short-term, shock-wave dynamics controlled (initial) Phase 1; (b) a relatively-longer, composite-laminate material deformation/damage/failure controlled (intermediate) Phase 2; and (c) a structural-vibration dominated (final) Phase 3. After the introduction of the nomenclature

used in the present work, the three projectile/composite-laminate interaction phases are analyzed in greater detail in the remainder of this section.

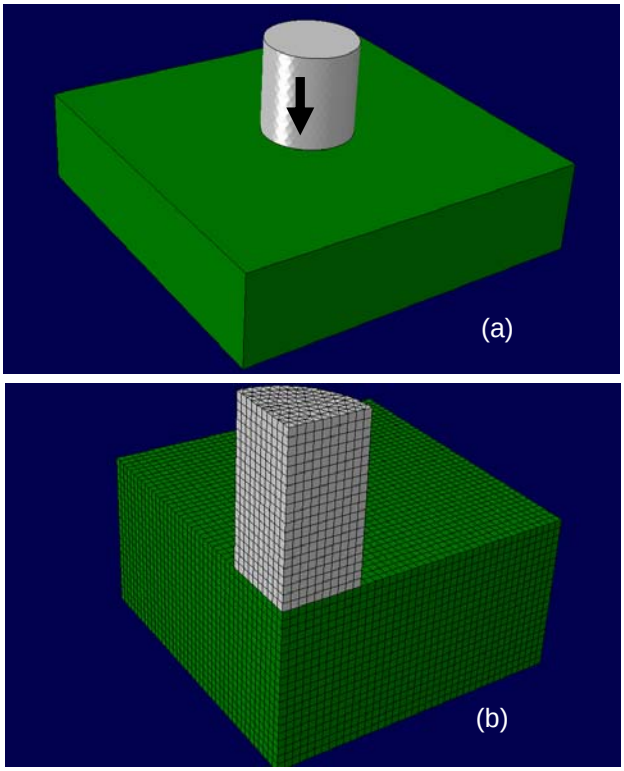

FIG. 3 (A) A SCHEMATIC OF THE PROBLEM INVOLVING A NORMAL (ZERO OBLIQUITY ANGLE) IMPACT OF A (SOLID, RIGHT CIRCULAR CYLINDER) PROJECTILE ONTO A THICK-SECTION COMPOSITE-LAMINATE TARGET STRUCTURE; AND (B) THE CORRESPONDING ONE-QUARTER FINITE ELEMENT MODEL USED IN THE NUMERICAL ANALYSIS OF THE COMPOSITE-LAMINATE BALLISTIC RESISTANCE LIMIT.

Nomenclature

V_i projectile incident velocity

m mass

A cross-sectional area

H (projectile) length or (composite-laminate) thickness

mass density

u material-particle velocity

$E^{el}_{33,comp}$ (uniaxial-strain) through-the-thickness elastic stiffness coefficient

C through-the-thickness shock (more accurately, acoustic wave) speed = ($E^{el}_{33,comp}$ /

$E^{pl}_{33,comp}$ (uniaxial-strain) through-the-thickness plastic tangent coefficient

z through-the-thickness shock/acoustic impedance (is equal to C_3)

through-the-thickness stress

$_y$ (uniaxial-strain) yield strength

Subscripts *proj* and *comp* denote projectile and composite-laminate related quantities.

Superscripts 0, *el* and *pl* stand for initial, elastic and plastic respectively.

A Short-term, Shock-wave Dynamics Controlled Phase 1

Within this phase of projectile/composite-laminate interaction, one can distinguish two distinct stages of interactions: (a) the initial stage within which the projectile impacts the composite-laminate target and gives rise to the generation of shocks within the projectile and target; and (b) the stage within which the projectile/composite-laminate interaction is controlled by the arrival of the release wave(s) (generated at the projectile back-face/free surface) to the projectile/composite-laminate interface. These two interaction stages are discussed separately below.

1) Impact stage

Within this stage of projectile/composite-laminate Phase 1 interaction, a backward-propagating (compressive) planar shock is generated within the projectile, while forward-propagating (compressive) shock(s) are generated within the composite-laminate. To simplify the analysis, shock(s) within the composite-laminate are assumed to be planar and longitudinal. Due to differences in the geometry (specifically, in the lateral dimensions) of the projectile and the composite-laminate, different stress states are produced by the backward and forward propagating shocks. That is, the back-propagating shock produces a uniaxial stress state while the forward propagating shock(s) give rise to a uniaxial-strain stress state.

Within this stage of projectile/composite-laminate Phase 1 interaction, two distinct impact-severity dependent regimes can be identified: (a) a purely-elastic regime which is encountered in cases when the through-the-thickness stress within the composite-laminate is smaller than the composite-laminate uniaxial-strain yield strength; and (b) an elastic-plastic regime which is encountered in cases when the through-the-thickness stress within the

composite-laminate exceeds the composite-laminate uniaxial-strain yield strength. Simple schematics are given in Figures 4(a)–(b) to clarify the two regimes of the impact stage of Phase 1 of projectile/composite-laminate interaction. It should be noted that, in the present work, it is assumed that the projectile is made of a sufficiently hard material so that, during impact, it can undergo only an elastic deformation.

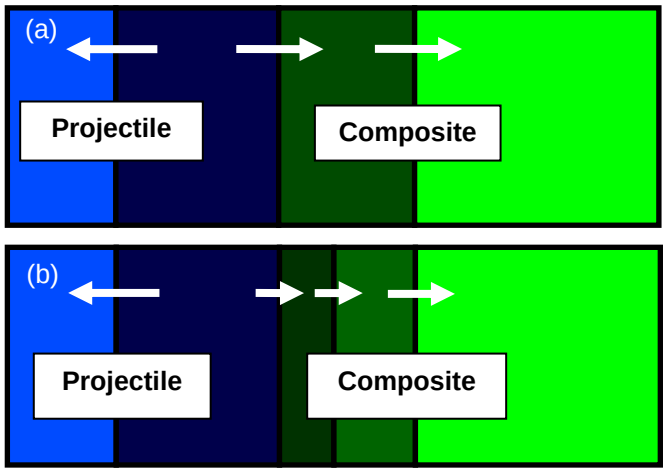

FIG. 4 SCHEMATICS OF TWO REGIMES WITHIN THE SHOCK-WAVE DYNAMICS CONTROLLED PHASE 1 OF THE PROJECTILE/COMPOSITE-LAMINATE INTERACTION PROCESS: (A) PURELY-ELASTIC REGIME; AND (B) ELASTIC-PLASTIC REGIME.

Purely-Elastic Regime: Within this regime, impact between the projectile and the composite-laminate results in the formation of two (elastic) shock waves, one in each of the interacting components. As mentioned earlier, in the projectile, the shock wave propagates in a direction opposite to the incident-direction of the projectile, while in the composite-laminate, the shock propagates in the projectile incident-direction. The continuity conditions for the through-the-thickness material-particle velocity and stress at the projectile/composite-laminate interface can then be respectively expressed as:

$$V_i - u_{proj} = u^{el}_{comp} \tag{1}$$

$$\begin{aligned} \sigma_{33,proj} &= z_{3,proj} * u_{proj} \\ &= \sigma^{el}_{33,comp} \\ &= z^{el}_{3,comp} * u^{el}_{comp} \end{aligned} \tag{2}$$

Through the combination of Eqs. (1) and (2), the following relations are obtained:

$$u^{el}_{comp} = \frac{z_{3,proj}}{\left(z_{3,proj} + z^{el}_{3,comp}\right)} V_i \tag{3}$$

$$\sigma^{el}_{33,comp} = \frac{z_{3,proj} * z^{el}_{3,comp}}{z_{3,proj} + z^{el}_{3,comp}} V_i = \sigma_{33,proj} \tag{4}$$

It should be noted that, within the analysis carried out in this section, as well as that in the remaining sections, the following assumptions are made (in addition to the one listed above): (a) both the projectile and the composite-laminate are assumed to be initially stress free; (b) the composite laminate is assumed to be initially stationary, while the projectile is moving at a velocity V_i; (c) only the normal (zero obliquity angle) projectile/composite-laminate impact is considered; (d) (elastic) material non-linearities are ignored, i.e. the elastic-shock speed is approximated with the corresponding (constant) acoustic-wave speed. The elastic-shock speeds are calculated as the square root of the ratio between the through-the-thickness stiffness coefficient and the material reference mass density. The projectile is assumed to undergo uniaxial-stress type of deformation and consequently, its through-the-thickness elastic stiffness coefficient is set equal to its Young's modulus. On the other hand, the composite-laminate is assumed to undergo a uniaxial-strain deformation and, hence, its through-the-thickness elastic stiffness coefficient is set equal to the 33-element of its elastic stiffness matrix (C33), where x_3 is taken to be the laminate through-the-thickness direction; (e) plastic response of the composite-laminate material is assumed to be of a linear-hardening character; and (f) all the shock-wave velocities are of the Lagrangian type i.e., they are defined relative to the (treated as being at rest) material in front of the shock.

Elastic-Plastic Regime: Within this regime, impact between the projectile and the composite-laminate results in the formation of two elastic shock waves and one plastic shock wave. An elastic back-propagating shock wave is formed within the projectile, as in the elastic regime, while a leading, elastic and a trailing, plastic forward-propagating shock waves are formed within the composite-

laminate. Within the composite-laminate, the elastic shock raises the through-the-thickness-stress to a level equal to the composite uniaxial-strain yield strength. The plastic shock on the other hand further raises the stress level to a value equal to that at the projectile/composite-laminate interface.

Since the stress-jump associated with the composite-laminate elastic shock is known (and equal to the corresponding uniaxial-strain yield strength), the state of the material produced by the passage of the elastic shock can be readily determined. That is, from Eq. (4), one can determine the material particle-velocity behind the elastic shock as:

$$u_{comp}^{el} = \frac{\sigma_{\mathrm{y}}}{z_{3,comp}^{el}} \tag{5}$$

From the fact that the composite-laminate undergoes uniaxial-strain deformation, material mass-density can be related to the composite-laminate through-the-thickness strain, $\varepsilon_{33,comp}^{el}$ as:

$$\rho_{comp}^{el} = \frac{\rho_{comp}^{0}}{1-\varepsilon_{33,comp}^{el}} = \frac{\rho_{comp}^{0}}{1-\dfrac{\sigma_y}{E_{33,comp}^{el}}} \tag{6}$$

As far as the state of the composite-laminate material behind the plastic shock is concerned, it is defined by the following state variables: ρ_{comp}^{pl}, u_{comp}^{pl}, $C_{3,comp}^{pl}$ and $\sigma_{33,comp}^{pl}$.

The afore-mentioned four state variables are defined by a set of four equations given below:

ρ_{comp}^{pl}, is defined by a relation analogous to Eq. (6) as:

$$\rho_{comp}^{pl} = \frac{\rho_{comp}^{0}}{1-\varepsilon_{33,comp}^{el}-\varepsilon_{33,comp}^{pl}} = \frac{\rho_{comp}^{0}}{1-\dfrac{\sigma_{33,comp}^{pl}}{E_{33,comp}^{el}}-\dfrac{(\sigma_{33,comp}^{pl}-\sigma_y)}{E_{33,comp}^{pl}}} \tag{7}$$

The mass and momentum conservation conditionsat the plastic-shock front, provide the following two additional relations between the four unknown state variables:

$$\rho_{comp}^{pl}\left(\left(u_{comp}^{pl}-u_{comp}^{el}\right)-C_{3,comp}^{pl}\right) = -\rho_{comp}^{el}C_{3,comp}^{pl} \tag{8}$$

$$\sigma_{33,comp}^{pl}-\sigma_y = \rho_{comp}^{el}\left(u_{comp}^{pl}-u_{comp}^{el}\right)C_{3,comp}^{pl} \tag{9}$$

The remaining fourth equation is obtained by combining the stress-equality relation at the projectile/composite-laminate interface:

$$\sigma_{33,comp}^{pl} = \sigma_{33,proj} = z_{3,proj} * u_{proj} \tag{10}$$

with the velocity-equality relation, at the same interface:

$$V_i - u_{proj} = u_{comp}^{pl} \tag{11}$$

to get:

$$\sigma_{33,comp}^{pl} = z_{3,proj} * (V_i - u_{comp}^{pl}) \tag{12}$$

Thus, Eqs. (7)–(9) and (12) defines a set of four equations relating the four unknown material state variables behind the plastic shock within the composite laminate. The four equations can be readily solved to obtain the values of the four state variables at a given level of the projectile incident velocity. An example of the results obtained using this procedure is shown in Figure 5, in which the through-the-thickness stress is plotted as a function of the projectile incident velocity. The values of the projectile and composite-laminate material parameters used in the construction of Figure 5 are provided in the caption of this figure. Examination of the results shown in Figure 5 reveals that up to the projectile velocity of ca. 185 m/s, the response of the composite-laminate to the impact is purely elastic while, at higher values of the projectile incident velocity, the response is of an elastic-plastic character. It should be noted that, at a given level of the projectile incident velocity, the stress value as displayed in Figure 5 corresponds to the maximum value of the projectile/composite-laminate interfacial normal stress (i.e., as will be shown below, subsequent projectile/composite-laminate interactions result in a decrease of this quantity).

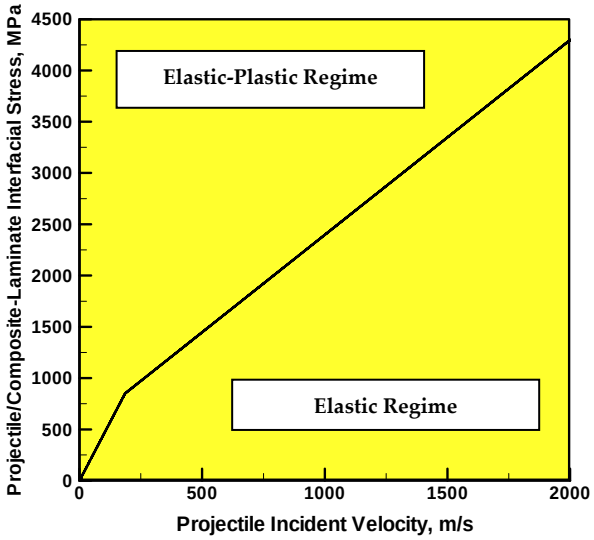

FIG. 5 VARIATION OF THE PROJECTILE/COMPOSITE-LAMINATE INTERFACIAL NORMAL STRESS WITH THE PROJECTILE INCIDENT VELOCITY. PROJECTILE PROPERTIES: $E_{proj} = 210\,GPa$, $\rho_{proj} = 7850\,kg/m^3$; COMPOSITE-LAMINATE PROPERTIES: $E^{el}_{33,comp} = 14.21\,GPa$, $\rho^0_{comp} = 1870\,kg/m^3$, $\sigma_y = 850\,MPa$, $E^{pl}_{33,comp} = 2.5\,GPa$.

When constructing Figure 5, one must account for the fact that the composite-laminate yield strength is a (plastic) strain-rate dependent quantity. This rate dependency is generally accounted for using the following relation:

$$\sigma_y(\dot{\varepsilon}^{pl}_{33,comp}) = \sigma_y\left(1 + B^{pl}_{33,comp}\ln\left(\frac{\dot{\varepsilon}^{pl}_{33,comp}}{\dot{\varepsilon}^{0,pl}_{33,comp}}\right)\right) \quad (13)$$

where, $B^{pl}_{33,comp}$ is an experimentally determinable material-dependent parameter, while $\dot{\varepsilon}^{pl}_{33,comp}$ and $\dot{\varepsilon}^{0,pl}_{33,comp}$, are, respectively, the current and a reference effective plastic strain rate (the latter is typically set to $1s^{-1}$). Determination of the effective plastic strain rate $\dot{\varepsilon}^{pl}_{33,comp}$ is a challenging task, since the (constant) plastic strain behind the forward-propagating plastic shock is built up (from a zero value, ahead of the shock), over the (unknown, a priori) shock-front width. To make things even more complicated, the shock-front width decreases (while the plastic strain increases) with an increase in the projectile incident velocity. Using a simple projectile/composite-laminate impact finite-element computational analysis (the results will be reported in a future communication), a relationship was established between the plastic-shock front width and the projectile incident velocity. By dividing this shock-front width with the shock speed, one can determine the time period over which the plastic strain attains its behind-the-shock constant value. Then the associated plastic strain rate is obtained by simply dividing the plastic strain with this time period.

2) Stage controlled by interaction of waves with the interface

Due to the fact that the projectile-material stiffness is substantially higher than the through-the-thickness composite-laminate elastic stiffness and due to a relatively large thickness of the composite-laminate, one generally finds that the backward-propagating shock wave within the projectile will reach the projectile free-end and the resulting forward-propagating decompression/release wave will reach the contact projectile/composite-laminate interface before the same sequence of events occurs within the composite laminate. In fact, one generally observes several shock wave reverberation cycles within the projectile before the release wave generated at the composite-laminate free-surface reaches the projectile/composite-laminate interface. Since the waves propagating within the projectile are all of an elastic character and due to the linear nature of the projectile-material constitutive response (which results in a constant wave speed), the duration of a single wave-reverberation cycle (within which a compressive shock-wave travels from the projectile/composite-laminate interface to the projectile free-surface and back) is constant and equal to:

$$\tau_{\text{cycle}} = \frac{2H_{proj}}{C_{3,proj}} \quad (14)$$

The (forward propagating) release wave, generated at the projectile back face, removes the (axial) stress within the projectile and lowers the material-particle velocity from $V_i - u_{proj}$ to $V_i - 2{*}u_{proj}$. When the release wave arrives at the projectile/composite-laminate interface, it is partially transmited to the composite laminate as a release wave, and partially reflects back into the projectile as a (compressive) shock wave. This process lowers the stress at, and the velocity of, the projectile/composite-laminate interface. The reflected shock wave within the

projectile then begins to propagate in the backward direction, initiating the second wave-reverberation cycle. At the end of the second cycle, interfacial stress and velocity again experience a decrease and the sequence of events described above repeats until the end of Phase 1 of projectile/composite-laminate interaction.

To determine the interfacial stress and velocity at the beginning of a new reverberation cycle (k+1, k=1, 2,…,and k=1 corresponds to the impact stage), the following procedure is utilized: It is first assumed that the projectile and the composite-laminate will remain in contact and that the material-particle velocity and stress continuity conditions will remain to be satisfied at the interface. The combined velocity/stress continuity condition is then expressed as:

$$\begin{aligned}\sigma_{33,proj}^{(k+1)} &= z_{3,proj} * u_{proj}^{k+1} \\ &= \sigma_{33,proj}^{(k)} - \left(z_{3,comp}^{el} * \left(u_{proj}^{k} + u_{proj}^{k+1}\right)\right)\end{aligned} \quad (15)$$

The second equality in Eq. (15) defines a single equation with one unknown, u_{proj}^{k+1}, and, hence can be readily solved. Then, using the first equality in Eq. (15), one can update the interface stress, $\sigma_{33,proj}^{(k+1)}$. Next, the interface velocity can be updated as:

$$u_{comp}^{pl,k+1} = u_{comp}^{pl,k} - \left(u_{proj}^{k} + u_{proj}^{k+1}\right) \quad (16)$$

The advancement of the projectile/composite-laminate interface within the reverberation cycle k, can be obtained by multiplying $u_{comp}^{pl,k}$ and τ_{cycle}. Using the procedure described above, an interfacial stress vs. interface location is generated in Figure 6 for the same projectile and the composite-laminate material and geometrical properties, and for the projectile incident velocity of 200 m/s. Examination of Figure 6 reveals that, as expected, the interfacial stress decreases with reverberation cycle, i.e. with the advancement of the projectile/composite-laminate interface. In addition, it is seen that the interfacial stress changes discontinuously between the reverberation cycles. It should be recognized that, in reality, this change occurs over a finite time period (the time period required for the interfacial velocity and stress continuity conditions to be re-established, after these continuity conditions were disrupted by the arrival of a release wave to the interface). Since our companion finite-element analysis established that this time period is small relative to the wave-reverberation cycle time, it was set to zero in the present work. Further examination of Figure 6 reveals that, while the duration of each reverberation cycle is the same, the incremental advancement of the projectile/composite-laminate interface decreases with the cycle number. This finding is consistent with the fact that the interfacial velocity decreases with an increase in the cycle number.

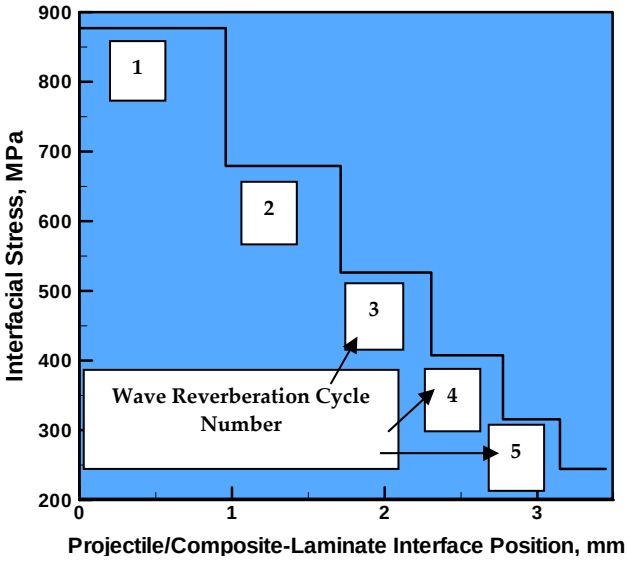

FIG. 6 VARIATION OF THE PROJECTILE/COMPOSITE-LAMINATE INTERFACIAL NORMAL STRESS WITH THE PROJECTILE/ COMPOSITE-LAMINATE INTERFACE LOCATION (AND THE WAVE-REVERBERATION CYCLE NUMBER) FOR THE CASE OF THE PROJECTILE INCIDENT VELOCITY OF 200 m/s AND THE PROJECTILE LENGTH OF 13.9 mm. THE PROJECTILE AND THE COMPOSITE-LAMINATE PROPERTIES USED ARE THE SAME AS THOSE LISTED IN THE CAPTION OF FIGURE 5.

Using the procedure described above, a plot of the projectile resistive force vs. the interface advancement, depicted in Figure 7 (a), is obtained for the combination of the projectile and composite-laminate material and geometrical parameters identical to the one used in the next (Phase 2) section. The projectile resistive force (i.e. the projectile/interface contact force) is obtained by multiplying the corresponding interfacial stress by the projectile cross-sectional area. The remaining details regarding the generation of Figure 7(a) are presented in the next section. It should be noted that while constructing Figures 6 and 7(a), no consideration was given to the possibility of arrival of the release wave (generated at the composite-laminate back-face) to the projectile/composite-laminate interface.

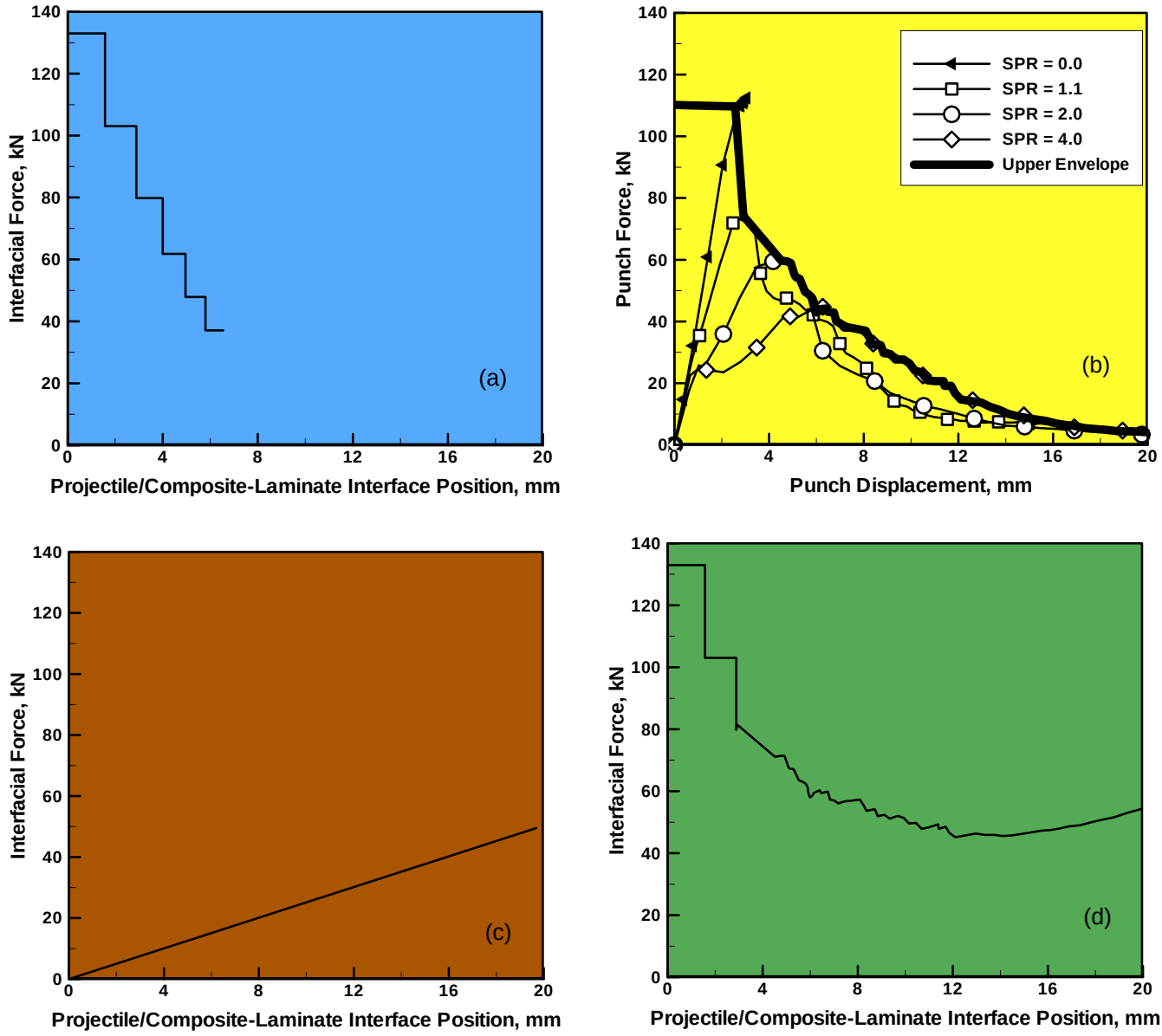

FIG. 7 INTERFACIAL FORCE VS. PROJECTILE/COMPOSITE-LAMINATE INTERFACIAL DISPLACEMENT IN: (A) PHASE 1; (B) PHASE 2, DENOTED BY THE HEAVY SOLID CURVE AND LABELED "*Upper Envelope*"; AND (C) PHASE 3 OF THE PROJECTILE/COMPOSITE-LAMINATE INTERACTION PROCESS. THE INTERFACIAL FORCE VS. PROJECTILE/COMPOSITE-LAMINATE INTERFACIAL DISPLACEMENT RELATION SPANNING ALL THREE INTERACTION PHASES IS SHOWN IN (D).

3) Stage controlled by interaction of waves with the interface

As mentioned earlier, this projectile/composite-laminate interaction phase comprises three distinct stages: (a) an initial stage of projectile penetration, which is characterized by large through-the-thickness shear in the presence of high hydrostatic compression; (b) a "*shear-plug*" formation stage within which through-the-thickness shear takes place in the presence of nearly uniaxial compression; and (c) a stage within which through-the-thickness shearing continues but the hydro-dynamic component of the stress field becomes tensile. Also, as recommended by Gama and Gillespie (2008) and Haque and Gillespie (2012), insight into the evolution of composite-laminate material deformation, damage and failure can be gained, and the associated projectile/composite-laminate interaction force can be assessed by carrying out a series of quasi-static punch-shear test at different values of the span/punch-diameter ratio. Specifically, Gama and Gillespie (2008) and Haque and Gillespie (2012) suggested that the interaction force vs. projectile displacement relation for Phase 2 can be defined as the upper envelope of the corresponding punch force vs. punch

displacement curves obtained at different values of the span/punch-diameter ratio. An example of such a curve is presented in Figure 7(b). It should be noted that the punch force vs. punch displacement curve associated with the span/punch-diameter ratio of 8.0 was excluded from the formulation of the upper-envelope curve since, at this value of the span/punch-diameter ratio, mechanical response of the composite laminate is bending rather than shear dominated. The punch force vs. punch displacement curve corresponding to the span/punch-diameter ratio of 8.0 will be analyzed in the next section.

4) Structural Vibration Controlled Phase 3

As mentioned earlier, within this projectile/composite-laminate interaction phase, the projectile/laminate assembly, in the case of partial penetration, or a composite-laminate alone, in the case of full penetration, vibrates until the vibrational energy is dissipated through structural and/or material damping. Since the main objective of the present work is the prediction of composite-laminate ballistic limit, the vibrational behavior of the same laminate is of less concern. However, following the suggestion of Gama and Gillespie (2008) and Haque and Gillespie (2012), an analysis of this phase enables assessment of the inertia/elastic-deformation contributions to the projectile resistive force. Specifically, Gama and Gillespie (2008) and Haque and Gillespie (2012), suggested that the punch peak force associated with a large value (e.g. = 8.0) of the span/punch-diameter ratio can be used as an upper-limit estimate of this contribution. This suggestion was based on the following observations: (a) as the projectile penetrates the laminate, the surrounding composite-laminate material exerts inertia and elastic-deformation resistive forces onto the projectile. It should be noted that these forces have not yet been accounted for in the present simple semi-empirical model; (b) at the point of maximum outward deflection of the laminate (back-face), the associated kinetic energy of the surrounding composite-laminate material is completely converted into the composite-material elastic-strain energy; and (c) in the case of bending controlled punch-shear tests under a large value of the span/punch-diameter ratio, the composite-laminate maximum deflection is associated with its punch peak force.

Following the suggestion of Gama and Gillespie (2008) and Haque and Gillespie (2012), a linear inertial/elastic/deformation force vs. forward advancement of the projectile relation is assumed. In this relation, the force is zero at the projectile advancement equal to zero. The force assumes a peak value (equal to the punch peak force at the span/punch-diameter ratio of 8.0) at the value of projectile advancement at which the projectile has exited/fully-penetrated the composite laminate. The resulting force vs. displacement plot is depicted in Figure 7(c).

5) Overall Interfacial Force vs. Interfacial Displacement Relationship

The procedure described in the previous sections, enabled establishment of the interfacial force vs. interfacial displacement relations in different interaction phases as well as the assessment of different components of the interfacial force. What is needed now is a procedure for determination of the force vs. displacement relationship which spans over the entire projectile/composite-laminate interaction process. Such a procedure, developed in the present work, involves the following two steps: (a) to account for the combined contributions of the composite-laminate material plastic deformation, damage, failure, inertial and elastic deformation effects, interfacial forces displayed in Figures 7(b)-(c) are first summed; and (b) at each value of the projectile/composite-laminate interface displacement, the combined punch-shear force obtained from (a) is compared with the corresponding interfacial force displayed in Figure 7(a) and the larger of the two forces is taken to represent the "controlling" interfacial force. The procedure just described yielded the interfacial force vs. interfacial displacement relationship depicted in Figure 7(d).

6) Prediction of the Composite-Laminate Ballistic Limit

Now that the interfacial force vs. interfacial displacement relation is known, one can proceed with the assessment of the composite-laminate ballistic limit (as represented by V_{50}). This can be simply done by equating the projectile incident kinetic energy associated with V_{50} with the work done by the projectile in overcoming the resistive force as defined by the plot in Figure 7(d). It should be noted that in Figure 7(d), the projectile/composite-laminate interface position of

19.68 mm corresponds to the condition of complete penetration of the laminate by the projectile. When the procedure described above is applied to the case at hand, V_{50} ~ 448.43 m/s is obtained. To validate the present model, a series of transient non-linear dynamic finite element analyses of the same projectile/composite-laminate impact problem is carried out in the next section. These (computationally intensive) analyses yielded, what would be generally considered, a more accurate assessment of V_{50} (since a smaller number of assumptions had to be made and a fairly comprehensive material model for the composite-laminate had to be used).

Validation of the Model

In this section, the same problem analyzed in the previous section is investigated using a series of transient non-linear dynamics finite element calculations, in which different values are assigned to the projectile impact velocity. The main objective of these calculations was the determination of V_{50} which can be used to validate the simple, semi-empirical model developed in the previous section. In the remainder of this section, a brief description is first given of the finite element procedure employed. This is followed by an overview of the results obtained and by a brief discussion of the findings regarding the validity/reliability of the proposed simple, semi-empirical model.

Finite element Model and Analysis

1) Problem Definition

The basic problem analyzed in the present work involves normal (zero obliquity angle) impact of a right circular cylinder, steel projectile (diameter = 12.5 mm, height=12.5 mm) onto a prototypical (balanced) plain-weave S2-glass fiber reinforced polyvinyl-ester-epoxy matrix (square-shaped) composite laminate (edge length = 50 mm, thickness = 12.5 mm). To address this problem using the finite-element approach, the following tasks had to be completed: (a) generation of the geometrical model; (b) generation of the mesh model; (c) assignment of the initial conditions; (d) assignment of the boundary conditions; (e) identification of contact surfaces and specification of contact algorithm; (f) definition of the material constitutive models; and (g) identification and application of the computational procedure. Each of these aspects of the present work is discussed in some details in the remainder of this section. It should be noted that for the problem analyzed in this section, the proposed simple semi-empirical model yielded V_{50} = 448.43 m/s.

2) Geometrical Model

A schematic of the geometrical model investigated in the present work is depicted in Figure 3(a). To take advantage of the intrinsic symmetry of the problem at hand, only one quarter of the model is explicitly analyzed (while the remaining quarters are accounted for through the use of the proper symmetry boundary conditions).

3) Meshed Model

The mesh model used in the finite element analyses of the projectile/composite-laminate interaction is depicted in Figure 3(b). It should be noted that, as explained above, the mesh model comprises only one quarter of the geometrical model. The mesh model for the projectile consists of 3240 six-node, first-order continuum elements while that for the composite-laminate consists of 32,000 eight-node, first-order reduced-integration continuum elements. Typical edge length of the two types of elements used is around 1.25 mm. The mesh size used was found to be a good compromise between accuracy and computational efficiency. In other words, further refinement in the mesh size was found to have minor effects on the numerical values of the results obtained and no effect on the nature of the findings and conclusions resulting from the present work.

4) Initial Conditions

The projectile and the composite laminate are assumed to be initially stress/strain free. Furthermore, the laminate is assumed to be initially stationary/quiescent while the projectile is assigned a constant initial velocity (in a 300–500 m/s range) in the negative z direction.

5) Boundary Conditions

With the exception of the symmetry boundary condition along the x=0 and y=0 planes, no additional boundary conditions were prescribed.

6) Contact/Interaction Conditions

Interactions between the projectile and the composite laminate are modeled using the "Hard Contact Pair" type of contact algorithm. Within this

algorithm, contact pressures between two bodies are not transmitted unless the nodes on the "slave surface" contact the "master surface". No penetration/over closure is allowed and there is no limit to the magnitude of the contact pressure that could be transmitted when the surfaces are in contact. Transmission of shear stresses across the contact interfaces is defined using a modified Coulomb friction law which utilizes the static/ kinetic friction coefficient and an upper-bound shear stress limit (a maximum value of shear stress that can be transmitted before shearing within the softer material, rather than interfacial sliding, begins to take place).

7) Material Models

Since the present model comprises two single-material components (projectile and composite laminate), there are only two materials whose mechanical constitutive response has to be addressed.

To comply with the non-plastically deforming projectile assumption (used in the development of the proposed simple semi-empirical model), the projectile is assumed to be made of steel, which is modeled as a linear-elastic isotropic material. Consequently, the projectile material is completely defined by its Young's modulus (E = 210 GPa), the Poisson's ratio (= 0.3) and the mass density (= 7850 kg/m^3).

Polymer-matrix Composite: As mentioned earlier, the target is assumed to be made of a prototypical (balanced) plain-weave S2-glass fiber reinforced composite-laminate material. Due to the balanced plain-weave nature of the reinforcing S2-glass fabric, this material is treated as a transversely isotropic material.

Before the material constitutive model for the composite laminate is defined, it should be noted that a material (mechanical) model defines, in general, relationships between the field/material-state variables (pressure/stress, mass-density/specific volume, energy-density, temperature, etc.). These relationships generally include: (a) an equation of state; (b) a strength model equation(s); and (c) a failure model equation(s). Partitioning of the material model into these three sets of equations is a natural consequence of the fact that the total stress tensor can be represented as a sum of a hydrostatic stress (scales with negative pressure) tensor (which causes a change in the volume/density of the material) and a deviatoric stress tensor (which is responsible for the shape change of the material). The hydrostatic part of the stress is defined by the equation of state which specifies the corresponding functional relationship between pressure, mass-density, and internal-energy density/temperature. The deviatoric part of the stress, on the other hand, is defined by the strength model which specifies the appropriate functional relations between the deviatoric-stress components and various field quantities quantifying the extent and rate of material deformation as well as the effect of material temperature. A failure model defines one or more stress-and/or strain-based conditions which, when attained, cause the material to fracture and lose its ability to support tensile normal and shear stresses.

It should be also noted that the separation of the total stress tensor into its hydrostatic part (as described by the equation of state) and its deviatoric part (as described by the strength model) enables proper modeling of the materials with respect to their ability to support shock and spreading waves. Specifically, as discussed in our prior work (Grujicic *et al.*, 2010b, c, d, e, 2012a, b, c); (a) shock-supporting normal materials must display material non-linearity of a type which yields an upward curvature in the associated pressure vs. specific volume (reciprocal of the density) plot (i.e., pressure increases at a continuously higher rate as the specific volume decreases); while (b) the anomalous materials must possess a downward curvature in the associated pressure vs. specific volume plot.

The hydrostatic response of the (balanced) plain-weave S2-glass fiber reinforced composite-laminate material is defined by an orthotropic equation of state in the form:

$$\begin{aligned} P = & -K_1 e_{vol} + K_2 e_{vol}^2 \\ & -\frac{1}{3}\left(C_{11}+C_{21}+C_{31}\right)e_{11}^d \\ & -\frac{1}{3}\left(C_{12}+C_{22}+C_{32}\right)e_{22}^d \\ & -\frac{1}{3}\left(C_{13}+C_{23}+C_{33}\right)e_{33}^d \end{aligned} \tag{17}$$

where $K_1 = \frac{1}{9}\left(C_{11} + C_{22} + C_{33} + 2\left(C_{12} + C_{23} + C_{31}\right)\right)$ is the effective bulk modulus, e_{vol} (scales linearly with $(\rho_{0/}\rho) - 1$, and are the density and reference density respectively) is the volumetric strain, K_2 is a coefficient in the quadratic non-linear correction to the relation P vs. e_{vol}, and the last three terms on the right hand side of Eq. (17) represent the contributions of the deviatoric strains, e_{ij}^{d} , to the pressure.

It should be noted that, due to an expected low extent of energy dissipation, no explicit dependence of pressure on the internal energy density is specified in Eq. (17). Values for all the parameters for the (balanced) plain-weave S2-glass fiber reinforced composite-laminate equation of state can be found in our recent work (Grujicic *et al.*, 2006).

As far as the strength model for the composite material is concerned, in order to make it consistent with the composite-laminate material model used in the development of the simple semi-empirical ballistic-limit model, it is assumed to be of a linear elastic and linear strain-hardening plastic character. The elastic part of the model is simply defined by a generalized Hooke's law which uses the orthotropic elastic stiffness matrix to map the deviatoric strain components to the corresponding deviatoric stress components. The components of the elastic stiffness matrix, C_{ij}, appearing in Eq. (17) and in the equation for K_1, are defined in terms of the corresponding engineering constants E_{ii}, G_{ij} and ν_{ij} (i,j=1,2,3) using standard relations. As far as the plastic part of the composite-laminate model is concerned, it is defined by: (a) a von-Mises (orthotropic) yield criterion; (b) a normality flow rule; and (c) a linear strain-hardening constitutive behavior. Values for all the parameters for the (balanced) plain-weave S2-glass fiber reinforced composite-laminate strength model can be found in our recent work (Grujicic *et al.*, 2006).

The failure model for the composite material used in the present work combines a failure initiation model with a material mechanical degradation model. Final failure is taken to occur when the material loses its ability to support any shear and/or tensile loads. The failure initiation model defines a stress or strain based criterion which when met leads to the onset of mechanical degradation of the material. Once failure is initiated, the strength and stiffness properties of the material are continuously updated in accordance with the extent of current level of material degradation. The material mechanical degradation model is based on the concept of cracked strain, ε_{cr} , which as it increases from the moment of failure initiation, gives rise to a progressive increase in the extent of material damage. The maximum value of each component of cracked strain is obtained using the computed or measured values of the associated failure stress and fracture energy. The fracture energies are determined experimentally using the double cantilever beam test (Riedel *et al.*, 2003).

Once the material has failed in a particular direction, the stress in that direction is set to zero while the stresses in the other directions are modified in accordance with the loss of Poisson's effect. When the failure occurs due to excessive tensile strains in the laminate through-the-thickness direction or due to excessive inter-lamellar shear strains, it is referred to as "delamination". On the other hand, laminate in-plane tensile stresses lead to "reinforcement" failure. When the material fails in more than one direction (the bulk failure) its properties are set to those of an equivalent isotropic material, and all tensile stresses are set to zero, while the shear stresses are set to a predefined residual shear stress level.

In addition to the stress/strain based failure criterion described above, matrix melting and/or fiber degradation due to excessive heating can also lead to material failure. Matrix melting occurs when the temperature exceeds the melting point of the polymer matrix and results in delamination failure mode. Fiber degradation occurs when the matrix temperature exceeds a predefined fiber degradation temperature and leads to a bulk mode of failure which leaves the material with an ability to support only compressive type of stresses. Based on the aforementioned description, the failure of the composite is controlled by three material-specific parameters, the crack strain ε_{cr}, the fracture energy G_f and the maximum stress at which the materials starts to degrade, $_{max}$. Values of all the parameters for the (balanced) plain-weave S2-glass fiber reinforced composite-laminate failure model can be found in our recent work (Grujicic *et al.*, 2007a).

8) Computational Procedure

All the calculations carried out in the present work were done using ABAQUS/Explicit (Dassault Systems, 2010) within which the problem at hand (formulated in terms of a set of mass, momentum and energy conservation differential equations along with the material constitutive relations, initial, boundary and contact/interaction conditions) is solved using a finite-element approach. A typical transient non-linear dynamics (quarter-model) finite-element analysis of impact of a right circular cylinder, steel projectile onto a prototypical (balanced) plain-weave S2-glass fiber reinforced polyvinyl-ester-epoxy matrix composite laminate required 10 minutes of (wall-clock) time on a 12 core, 3.0 GHz machine with 12 GB of memory.

It should be noted that no variable mass scaling algorithm was used to improve the computational efficiency due to the relatively low computational cost. Furthermore, due to the very fine nature of the mesh and the absence of strong shock waves, no bulk viscosity algorithm (aimed at mitigating the computational challenges associated with large field gradients) was used.

Results and Discussion

As mentioned earlier, the main purpose for carrying out a series of finite-element analyses dealing with the projectile/composite-laminate normal impact is to obtain a more accurate assessment of the composite/laminate ballistic limit, i.e., V_{50}. Nevertheless, before the finite element results pertaining to the ballistic-limit assessment are presented, few typical field plots will be shown and briefly discussed.

Examples of the typical results obtained in this portion of the work are shown in Figures 8(a)–(d) and 9(a)–(d). The results displayed in Figures 8(a)–(d) show the temporal evolution and spatial distribution of the projectile and the composite-laminate materials, while the ones displayed in Figures 9(a)–(d) show the corresponding temporal evolution and spatial distribution of the normal stress in the through-the-thickness direction within the composite-laminate. A brief examination of the results displayed in Figures 8(a)–(d) and 9(a)–(d) reveals that:

(a) As the projectile penetrates the composite-laminate, the composite-laminate material in front of and surrounding the projectile becomes highly deformed and damaged/fractured. This leads to the formation of an initial shear-plug. In addition, a bulge begins to form at the composite-laminate back-face;

(b) After the projectile has penetrated slightly more than half of the composite-laminate thickness, the back-face bulge begins to shear off. This process results in the formation of a detached slug which is pushed out by the advancing projectile; and

(c) As far as the composite-laminate through-the-thickness normal stress is concerned, its spatial distribution is dominated in the initial stages of the projectile/composite-laminate interaction by the propagation of compressive and decompression/tension shock waves (as evidenced by the presence of the high compressive < -50 MPa and high tensile stress > 500 MPa regions in Figure 9(a)).

The effect of the projectile initial velocity on the projectile residual velocity is depicted in Figure 10. It should be noted that the projectile incident velocity at which the residual velocity is zero is defined as V_{50} while a negative value of the residual velocity corresponds to the case of a rebounded/defeated projectile. Examination of the results displayed in Figure 10 shows that the composite-laminate ballistic limit predicted by the finite-element computational analysis is $V_{50} \sim 445$ m/s. This result is quite close to its counterpart (equal to 448.43 m/s) predicted by the proposed simple semi-empirical model. Since a similar level of agreement was obtained for a few additional simulations in which the projectile size and the laminate thickness were varied, it appears that the proposed simple semi-empirical model can provide a reliable prediction for the composite-laminate ballistic limit (under normal impact conditions and for the case of a solid right circular cylinder, plastically non-deformable projectile).

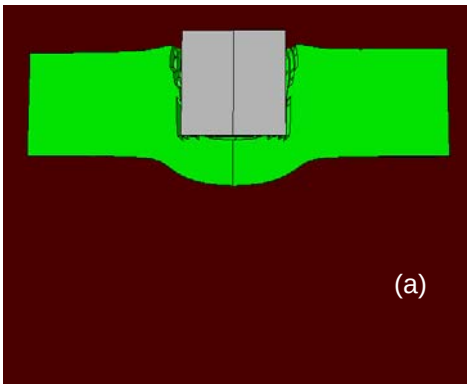

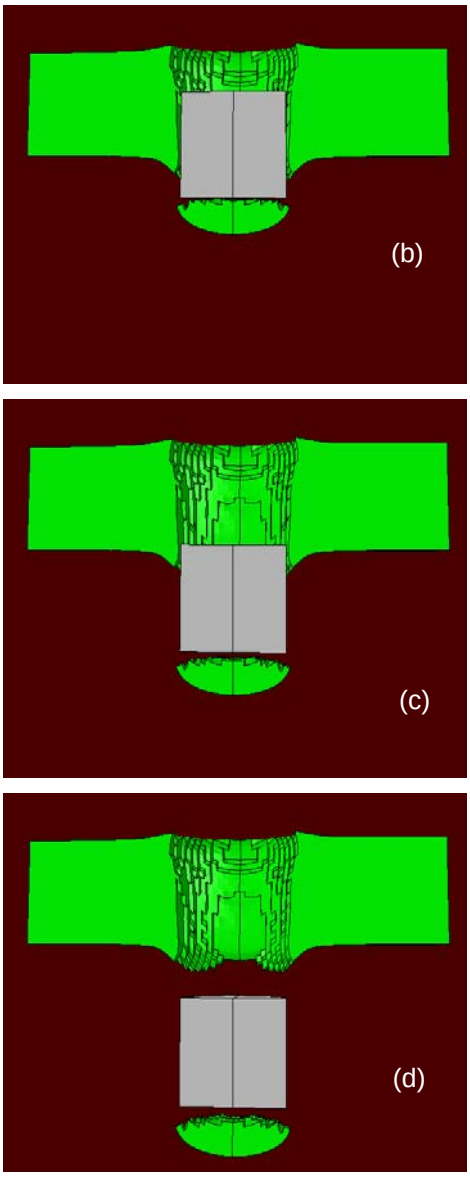

FIG. 8. SPATIAL DISTRIBUTION OF THE PROJECTILE AND THE COMPOSITE-LAMINATE MATERIAL AT FOUR POST INITIAL-IMPACT TIMES: (A) 75 μs; (B) 150 μs; (C) 225 μs; AND (D) 300 μs. PROJECTILE INITIAL VELOCITY IS EQUAL TO 350 m/s.

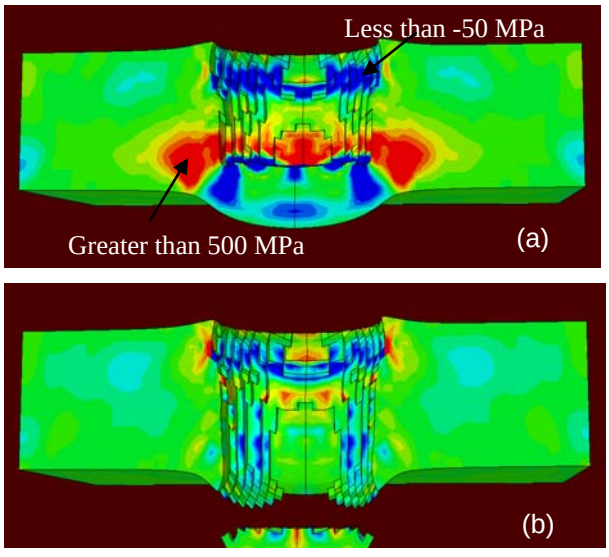

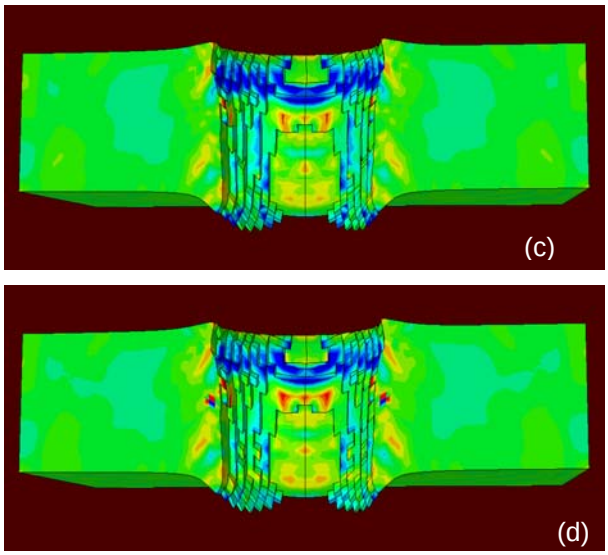

FIG. 9 SPATIAL DISTRIBUTION OF THE THROUGH-THE-THICKNESS COMPONENT OF THE STRESS WITHIN THE COMPOSITE LAMINATE AT FOUR POST INITIAL-IMPACT TIMES: (A) 75 μs; (B) 150 μs; (C) 225 μs; AND (D) 300 μs. PROJECTILE INITIAL VELOCITY IS EQUAL TO 350 m/s.

Summary and Conclusions

Based on the results obtained in the present work, the following main summary remarks and conclusions can be drawn:

1. A simple semi-empirical model for prediction of the ballistic-limit of thick-section composite laminates when subjected to a normal impact by a solid (right circular cylinder) plastically non-deformable projectile is developed.

2. Within the model, the projectile/composite-laminate interaction process is divided into three distinct phases. The initial Phase 1 is analyzed using the theory of planar, longitudinal shock-waves while the intermediate Phase 2 and the final Phase 3 are modeled using the experimental results (properly modified to include the dynamic effects) obtained in conventional quasi-static punch-shear tests.

3. Through the application of the model, a prediction is obtained for the composite-laminate ballistic limit (as quantified by V_{50}, i.e. a velocity at which the probability for full penetration of the composite laminate is 50%).

4. To validate the model, a companion series of transient non-linear dynamics finite-element analyses of the same normal-impact problem is carried out. These analyses have yielded another (more accurate) prediction for V_{50}.

5. Since a reasonable agreement is observed between

the two V_{50} predictions, it is suggested that the proposed simple semi-empirical model can provide a reliable assessment for the composite-laminate ballistic limit.

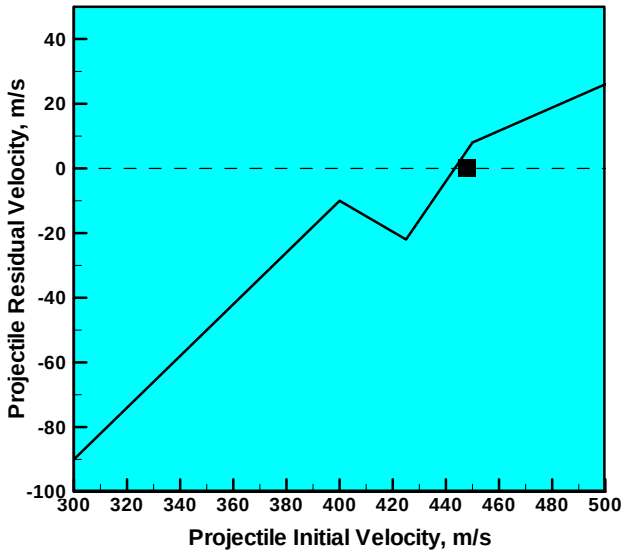

FIG. 10 EFFECT OF THE PROJECTILE INITIAL VELOCITY ON THE PROJECTILE RESIDUAL VELOCITY AS PREDICTED BY THE FINITE-ELEMENT CALCULATIONS (SOLID LINE). V_{50} CORRESPONDS TO THE PROJECTILE INITIAL VELOCITY AT WHICH THE RESIDUAL VELOCITY IS ZERO. THE CORRESPONDING V_{50} PREDICTED BY THE SIMPLE SEMI-EMPIRICAL MODEL IS SHOWN AS A BLACK-FILLED SQUARE.

REFERENCES

Bless, S. J., and D. R. Hartman, "Ballistic penetration of S-2 glass-laminates." In Proceedings of the 21st International SAMPE technical conference, Advanced Materials: the Big Payoff, edited by R. Wegman, H. Kliger, E. Hogan, 21 (1989): 852–866.

Dassault Systems, "ABAQUS Version 6.10, User Documentation", 2010.

Gama, B. A., and J. W. Gillespie, Jr., "Punch Shear Based Penetration Model of Ballistic Impact of Thick-Section Composites." Composite Structures, 86 (2008): 356–369.

Grujicic, A., M. LaBerge, M. Grujicic, B. Pandurangan, J. Runt, J. Tarter and G. Dillon, "Potential Improvements in Shock-Mitigation Efficacy of A Polyurea-Augmented Advanced Combat Helmet: A Computational Investigation," Journal of Materials Engineering and Performance, 21 (2012a): 1562–1579.

Grujicic, M., A. Arakere, B. Pandurangan, A. Grujicic, A. A. Littlestone and R. S. Barsoum, "Computational Investigation of Shock-Mitigation Efficacy of Polyurea when used in a Combat Helmet: A Core Sample Analysis," Multidiscipline Modeling in Materials and Structures, 8 (2012b): 297–331.

Grujicic, M., B. P. d'Entremont, B. Pandurangan, J. Runt, J. Tarter and G. Dillon, "Concept-Level Analysis and Design of Polyurea for Enhanced Blast-Mitigation Performance," Journal of Materials Engineering and Performance, 21 (2012c): 2024–2037.

Grujicic, M., B. Pandurangan, D. C. Angstadt, K. L. Koudela and B. A. Cheeseman, " Ballistic-Performance Optimization of a Hybrid Carbon-Nanotube /E-glass Reinforced Poly-Vinyl-Ester-Epoxy-Matrix Composite Armor." Journal of Materials Science, 42 (2007b): 5347–5359.

Grujicic, M., B. Pandurangan, K. L. Koudela, and B. A. Cheeseman, "A Computational Analysis of the Ballistic Performance of Light-Weight Hybrid-Composite Armor." Applied Surface Science, 253 (2006): 730–745.

Grujicic, M., B. Pandurangan, T. He, B. A. Cheeseman, C-F. Yen and C. L. Randow, "Computational Investigation of Impact Energy Absorption Capability of Polyurea Coatings via Deformation-Induced Glass Transition," Materials Science and Engineering A, 527 (2010e): 7741-7751.

Grujicic, M., B. Pandurangan, U. Zecevic, K. L. Koudela, and B. A. Cheeseman, "Ballistic Performance of Alumina/S-2 Glass Fiber-Reinforced Polymer-Matrix Composite Hybrid Light Weight Armor Against Armor Piercing (AP) and Non-AP Projectiles." Multidiscipline Modeling in Materials and Structures, 3 (2007a): 287–312.

Grujicic, M., G. Arakere and T. He, "Material Modeling and Structural Mechanics Aspects of Traumatic Brain Injury Problem." Multidisciplinary Modeling in Materials and Structures, 6 (2010b): 335–363.

Grujicic, M., G. Arakere, T. He, W. C. Bell, B. A. Cheeseman, C-F.Yen and B. Scott, "A Ballistic Material Model for Cross-Plied Unidirectional Ultra-High Molecular Weight Polyethylene Fiber-Reinforced Armor-Grade Composites." Materials Science and Engineering A, 498 (2008c): 231–241.

Grujicic, M., T. He, H. Marvi, B. A. Cheeseman and C.-F.Yen, "A Comparative Investigation of the Use of Laminate-

level Meso-scale and Fracture-mechanics Enriched Meso-scale Composite-material Models in Ballistic-resistance Analyses." Journal of Materials Science, 45 (2010a): 3136–3150.

Grujicic, M., W. C. Bell, B. Pandurangan, and P. S. Glomski, "Fluid/Structure Interaction Computational Investigation of the Blast wave Mitigation Efficacy of the Advanced Combat Helmet." Journal of Materials Engineering and Performance, 20 (2010d): 877–893.

Grujicic, M., W. C. Bell, B. Pandurangan, and T. He, "Blast Wave Impact-Mitigation Capability of Polyurea When Used As Helmet Suspension Pad Material." Journal of Materials and Design, 31 (2010c): 4050–4065.

Grujicic, M., W. C. Bell, L. L. Thompson, K. L. Koudela and B. A. Cheeseman, "Ballistic-Protection Performance of Carbon-Nanotube Doped Poly-Vinyl-Ester-Epoxy Composite Armor Reinforced with E-glass Fiber Mats." Materials Science and Engineering A, 479 (2008b): 10–22.

Grujicic, M., W. C. Bell, S. B. Biggers, K. L. Koudela and B. A. Cheeseman, "Enhancement of the Ballistic-Protection Performance of E-glass Reinforced Poly-Vinyl-Ester-Epoxy Composite Armor via the Use of a Carbon-Nanotube Forest-Mat Strike Face." Materials: Design and Applications, 222 (2008a): 15–28.

Haque, B. Z. and J.W. Gillespie, Jr, "A combined theoretical–semiempirical penetration model of ballistic penetration of thick section composites." Journal of Thermoplastic Composite Materials, 25 (2012): 631-659.

Riedel, W., D. M. White, R. A. Clegg, and W. Harwick, "Advanced Material Damage Models for Numerical Simulation Codes", EMI-Report No. I 75/03, ESA CR (P) 4379, October 2003.

Zhou, G., and G. A. O. Davies, "Impact response of thick glass fibre reinforced polyester laminates." International Journal of Impact Engineering, 16 (1995): 357–374.